Asymmetrical Body Shape: Inducing Locomotion in a Simply Activated Amoeboid Robot *

Steven Rich (sir2@rice.edu)

Supervisor: Utku Culha

September 24, 2013

*Bio-Inspired Robotics Lab, Institute of Robotics and Intelligent Systems, Department of Mechanical and Process Engineering, Eidgenössische Technische Hochschule Zürich

1 Introduction

Characterized by their amorphous and flexible form, amoeba, along with some other microorganisms, can move forward by changing their shape and extending a portion of their cytoplasm. They use this protrusion, called a pseudopodium, to pull the rest of their body forward in a crawling-type motion [1]. In robotics, the problem of amoeboid locomotion has been addressed in several ways. Umedachi approached the issue by coordinating a number of communicating robots around an air sac, meant to resemble the cytoplasm of a cell [2], while Ingram uses what he calls Whole Skin Locomotion, the continuous inversion of a toroid [3]. These methods, while very impressive and complex, are naturally quite heavy, both computationally and energetically. I wished to create a simpler form of locomotion that would employ instead the embodied intelligence of a robot to initiate forward motion.

Thus, I selected the simplest input I could find, a single DC motor rotating at a constant velocity, and manipulated the mechanical structure of the robot in order to move it consistently forward. Since motion in an amoeboid robot depends largely on the frictional interactions between the robot and the ground, this directional force was achieved by instituting anteroposterior (front-back) asymmetry. Different elasticities, coefficients of friction, and an eccentric center of mass, turned this constant, circular motion into alternately-stepping forward locomotion.

2 Prototypes

Two separate prototypes were constructed using similar designs and construction processes. Each model employed a soft material as a primary skeleton to permit the robot to deform, and thus move forward. Hot-melt adhesives (HMA) were selected as materials because of their flexibility, workability, availability, and economical pricing. They allowed the main body to bend, while maintaining a relatively high damping ratio to eliminate unwanted resonance. Furthermore, they could be connected or permanently deformed with a conventional hot glue gun, allowing for many models and trials in a relatively short period of time.

2.1 Initial Prototype

The first prototype (Fig. 1) was constructed as a proof-of-concept for a simple activation mode of amoeboid motion. It consisted of a ring formed from two half-sticks of the hot-melt adhesive (HMA) glued end to end and a single DC motor supported slightly eccentrically by two other sticks. A string was attached to the motor's rotating shaft, looped through an eyelet on one side of the ring, and tied to the HMA on the other side.

An applied voltage initiated a small rotation in the motor that wound the string around the shaft, pulling the two sides of the ring nearer. After several turns, the torque of the motor was be insufficient to continue to compress the ring, and the motor halted. The voltage was then removed, allowing the elastic ring to restore its original shape, returning the motor and string to their starting positions. This transfer between constant voltage and zero voltage was achieved by exploiting the natural vibration of the prototype in order to connect and disconnect the wires from the motor's leads. The resulting square wave input caused the rapid compression and relaxation of the HMA ring.

From this vibrating mode, forward motion was produced by utilizing a friction gradient between the front and the back of the prototype. The center of mass was located slightly rear of center, and the coefficient of friction on the front half was decreased by

means of a cloth foot. Additionally, a drop of HMA at the rear of the ring increased the backward friction without significantly contributing to the forward sliding friction.

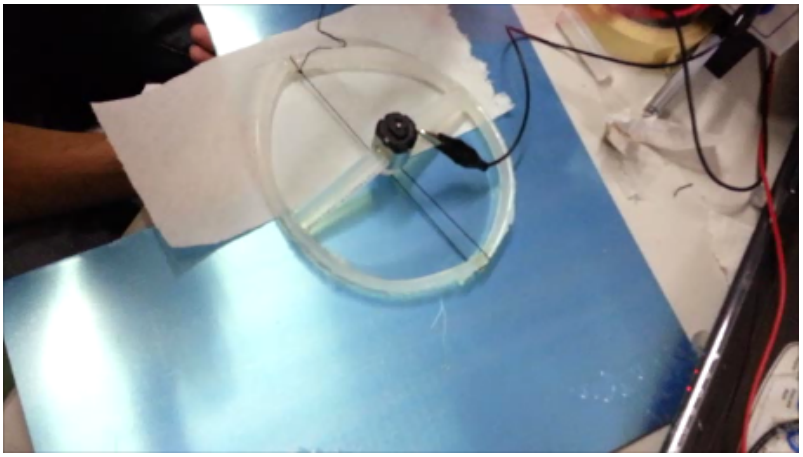

Figure 1: Prototype 1 on sliding surface

2.2 Final Prototype

The final prototype (Fig. 2) sought to solve some of the design problems that plagued the first prototype, including:

- Small step size
- Non-continuous input
- Twisting tendons
- Erratic motion

The second iteration had an HMA skeleton similar to that of the initial prototype (a DC motor supported by two HMA sticks in a ring of two bisected sticks). The motor, however, was connected to a gearbox that increased the torque of the shaft, and thus the force applied HMA ring. This enabled the HMA ring to compress, creating a step of up to 1.8 cm, compared to the sub-millimeter step of the first prototype. The gearbox shaft was attached to a 2.8 cm diameter wheel, with a small ball bearing (1 cm) connected near the edge. This new motor set-up simultaneously solved both the problem of the non-continuous input and the twisting tendon. Because the tendon was glued to this ball bearing, the rotation of the wheel did not twist the string as the ball bearing rotated naturally in the opposite direction. Additionally, the rotation of the wheel given a constant voltage was uniform, imparting a sinusoidal force input into the HMA ring, thanks to the radially located tendon attachment.

The resulting rotation caused a much larger compression in the HMA ring than in the initial prototype, leading to a much larger, but much slower step. A transverse asymmetry in weight distribution and friction coefficients created forward motion in a similar manner to the initial prototype. Because of the slower, larger, and more consistent step, however, the prototype moved faster and less erratically.

3 Modeling

After the constructing the prototypes, I sought to create a representative computer model of their motion to present the different forces at work, and gain an understanding of the relative importance of each customizable variable on the prototype. In both models, the robot was represented by a four mass system in a triangular configuration, with four spring-damper connections and one rigid connection. The top mass (Mass 1), which represented the motor, had an applied force from the tendon attachment and swung back and forth above the center mass (Mass 3) via an inverted pendulum. As the tendon also connected to Mass 2 and Mass 3, the tension force was applied to these two masses. Additionally, a frictional force was applied to all three masses in contact with the ground (Mass 2, Mass 3, and Mass 4). The free body diagram is presented below (Fig. 3). The resulting dynamic model yielded Newtonian equations of motion, which were input into MATLAB, and solved via various methods, until `ode45` was selected. Two separate simulations were created with this method. The differences between the two iterations of the computer models are expanded in the following sections.

3.1 Computer Model I

The first computer model consisted of two phases to represent the alternating sliding of the front and the back of the HMA ring. In the first phase, the leading edge of the ring remained stationary while the ring compressed, moving the back edge forward. In the second phase, the back edge was stationary while the leading edge advanced. The switching event used in `ode45` to change between these two phases was the arrival of the $\dot{x}$ at zero. Thus, every period of the sinusoidal force input (corresponding to one half-rotation of the motor wheel) represented a change between phases. In the model, the stationary edge was fixed by simply setting the acceleration to zero, instead of addressing the complex issue of static and sliding friction. This oversimplification was addressed in the second model. Several other issues plagued the first dynamic model, including:

- Exclusion of both sliding and static friction
- Improper constraints applied to the rigid body (constant length not maintained)
- Poorly selected spring and damping constants
- Neglected solver tolerance values

3.2 Computer Model II

Many of these issues identified in the first model were addressed and repaired when Model II was constructed. The static friction was included in the model first by eliminating the two-phase motion used in the first computer model and replacing it with a single set of equations containing a force-dependent binary friction term. If the force applied to each mass was less than the static friction value determined by $f_m N_m$, when f_m is the coefficient of friction for mass m and N_m is the associated normal force, the acceleration of the mass was set to 0. If the force applied was greater than the static friction value, the mass was in motion and a kinetic friction value (defined as $f_m N_m$ in the direction opposite the motion of the mass) was used. For mass 2, a directionality in the friction force was included by defining different coefficients of static friction for a negative or positive applied force. Thus, the variations in normal force created by the interactions between the masses created discrepancies in frictional forces that allowed the masses to alternate motion.

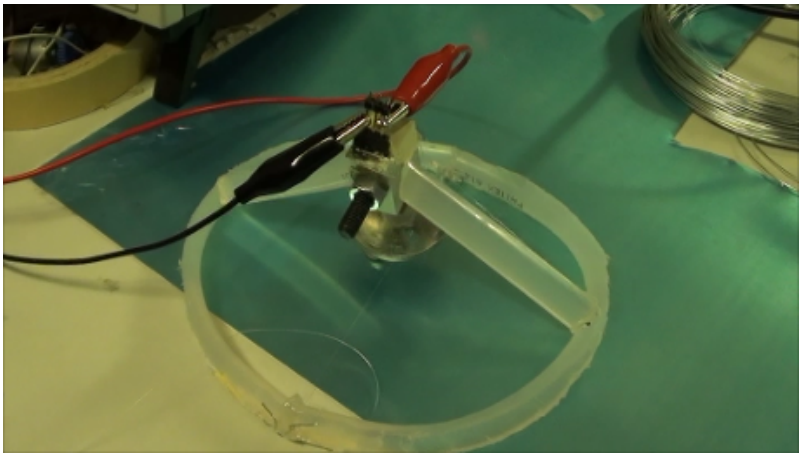

Figure 2: Final prototype attached to power source

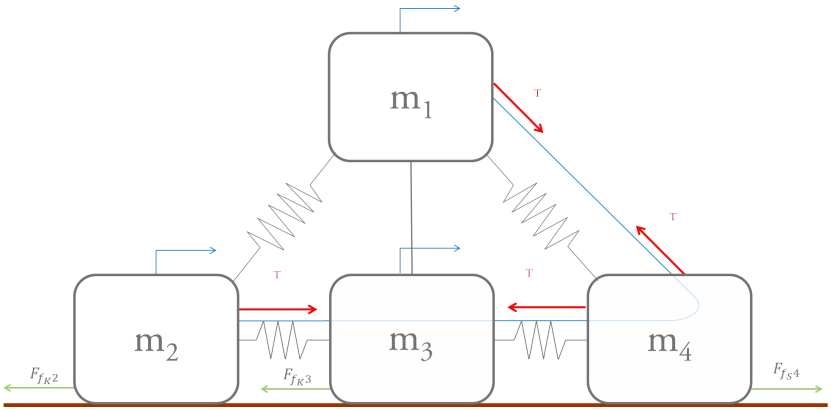

Figure 3: Free Body Diagram

The rigid body constraint was addressed with the inclusion of several compatibility equations. Thus, the equations of motion became:

$$
\begin{aligned}
m_1\ddot{x_1} &= F_p\sin\theta - F_{k1x} + F_{k2x} - F_{b1x} + F_{b2x} + T_x \\
m_1\ddot{y_1} &= F_p\cos\theta - F_{k1y} + F_{k2y} - F_{b1y} - F_{b2y} - F_{g1} - T_y \\
m_2\ddot{x_2} &= F_{k1x} + F_{k3x} + F_{b1x} + F_{b3x} + T - F_{F2} \\
m_2\ddot{y_2} &= F_{k1y} - F_{Fb1y} - F_{g2} + F_{N2} \\
m_3\ddot{x_3} &= -F_p\sin\theta - F_{k3x} + F_{k4x} - F_{b3x} + F_{b4x} - F_{F3} \\
m_3\ddot{y_3} &= -F_p\cos\theta - F_{g3} + F_{N4} \\
m_4\ddot{x_4} &= -F_{k2x} - F_{k4x} - F_{b2x} - F_{b4x} - T_x - T - F_{F4} \\
m_4\ddot{y_4} &= F_{k2y} + F_{b2y} - F_{g4} + T_y + F_{N4} \\
\ddot{x_1} &= \ddot{x_3} + h\left(\sin(\theta)\,\dot{\theta}^2 + \cos(\theta)\,\ddot{\theta}\right) \\
\ddot{y_1} &= \ddot{y_3} - h\left(\cos(\theta)\,\dot{\theta}^2 + \sin(\theta)\,\ddot{\theta}\right) \\
m_2\ddot{y_2} &= 0 \\
m_3\ddot{y_3} &= 0 \\
m_4\ddot{y_4} &= 0
\end{aligned}
$$

where F_p represents the unknown force applied by the rigid body, F_{kN} represents the spring force for spring N, F_{BN} represents the damping force for spring N, T represents the applied tension force, F_{gN} represents the gravitational force on mass N, F_{FN} represents the frictional force on mass N, F_{NN} represents the normal force for mass N, and x and y denote the x and y components of the respective forces.

In order to isolate the double-dot terms, the equations were separated into a matrix of known elements and unknown elements, each row relating to the relevant equations, and each column representing an unknown term. The known matrix is given by:

$$
K = \begin{bmatrix}
-F_{k1x} + F_{k2x} - F_{b1x} + F_{b2x} + T_\alpha \\
-F_{g1} - F_{k1y} - F_{k2y} - F_{b1y} - F_{b2y} - T_\alpha \\
F_{k1x} + F_{k3x} + F_{b1x} + F_{b3x} + T \\
F_{k1y} + F_{b1y} - F_{g2} \\
-F_{k3x} + F_{k4x} - F_{b3x} + F_{b4x} \\
-F_{g3} \\
-F_{k2x} - F_{k4x} - F_{b2x} - F_{b4x} - T_{x\alpha} - T \\
F_{k2y} + F_{b2y} - F_{g4} + T_{y\alpha} \\
-h\sin(\theta)\,\dot{\theta}^2 \\
-h\cos(\theta)\,\dot{\theta}^2 \\
0 \\
0 \\
0
\end{bmatrix}
$$

and the unknown matrix is given by:

$$G = \left[\begin{array}{cccccccc|ccccc} m_1 & 0 & 0 & 0 & 0 & 0 & 0 & 0 & 0 & 0 & 0 & 0 & -\sin\theta \\ 0 & m_1 & 0 & 0 & 0 & 0 & 0 & 0 & 0 & 0 & 0 & 0 & -\cos\theta \\ 0 & 0 & m_2 & 0 & 0 & 0 & 0 & 0 & 0 & f_2 & 0 & 0 & 0 \\ 0 & 0 & 0 & m_2 & 0 & 0 & 0 & 0 & 0 & -1 & 0 & 0 & 0 \\ 0 & 0 & 0 & 0 & m_3 & 0 & 0 & 0 & 0 & 0 & f_3 & 0 & \sin\theta \\ 0 & 0 & 0 & 0 & 0 & m_3 & 0 & 0 & 0 & 0 & -1 & 0 & \cos\theta \\ 0 & 0 & 0 & 0 & 0 & 0 & m_4 & 0 & 0 & 0 & 0 & f_4 & 0 \\ 0 & 0 & 0 & 0 & 0 & 0 & 0 & m_4 & 0 & 0 & 0 & -1 & 0 \\ 1 & 0 & 0 & 0 & -1 & 0 & 0 & 0 & -h\cos\theta & 0 & 0 & 0 & 0 \\ 0 & 1 & 0 & 0 & 0 & -1 & 0 & 0 & h\sin\theta & 0 & 0 & 0 & 0 \\ 0 & 0 & 0 & m_2 & 0 & 0 & 0 & 0 & 0 & 0 & 0 & 0 & 0 \\ 0 & 0 & 0 & 0 & 0 & m_3 & 0 & 0 & 0 & 0 & 0 & 0 & 0 \\ 0 & 0 & 0 & 0 & 0 & 0 & 0 & m_4 & 0 & 0 & 0 & 0 & 0 \end{array}\right]$$

These terms were then inserted into the output vector used in `ode45`, yielding a trajectory vector that gave both the initial values for the next time step and the subsequent motion of the model.

The spring and damping constants in the second model were determined by investigating the range of practical constraints given the characteristics of HMAs, and tuned to give the model the appropriate properties. These values were manually optimized by comparing graphs of the forces and selecting values that would improve performance after stability.

Inputting tolerance values into the solver prevented the longterm explosion of the model. A max step size of 3×10^{-3}, a relative tolerance of 1×10^{-5}, and an absolute tolerance of 1×10^{-8} were used. This stabilized the total energy of the system over time.

4 Results

The motion of the computer model reflects the basic motion of the robot, but some differences must be resolved before the model is realistic enough to permit accurate optimization. As with the prototype, the coefficients of friction play an essential role in the model's locomotion: without these differential characteristics, all the forces acting on the model are internal, and it simply oscillates in place. Unlike the actual model, however, the simulation employs no asymmetry in the mass balance. Similarly, the differences in damping and spring constants between front and back are neglected for this iteration.

In the actual model, the movement is characterized by a regular stepping motion, with the sliding of the front and back contacts separated into two distinct phases: a stationary front section coupled with an advancing back section, and an advancing front section coupled with a stationary back section. Neither of these phases contains any backward movement by either contact. The second computer simulation, however, does not represent these two phases distinctly, and although primary motion alternates between the front and the back section, there is a small amount of sliding in both directions by the "stationary" masses. This can be tuned by adjusting the coefficients of sliding and static friction, and most likely manipulating the mass balance as well as the spring and damping coefficients.

Additionally, the prototype began to move immediately with a regular step, requiring no apparent settling time to reach its final motion. The computer model, however, oscillated irregularly for several seconds before stabilizing into a regular motion. The delay before the masses converge to a constant velocity, illustrated by a linear position

function, is shown in Figure 4. Since all four masses are connected by relatively short springs, this graph of the leading mass (Mass 4), very nearly reflects the positions of the other three masses on such a relatively large position scale.

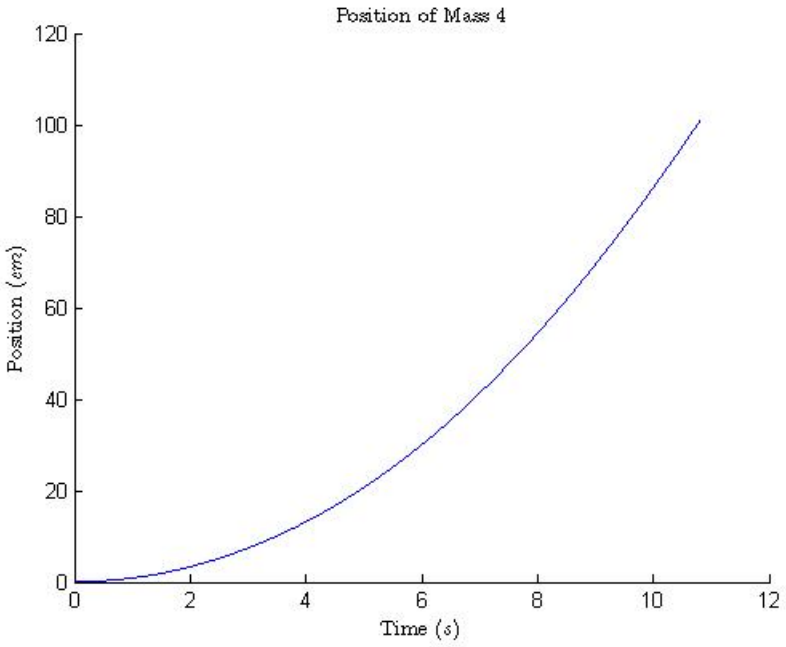

Figure 4: Position Graph of Mass 4

The final position function is also too steep, indicating a stable speed considerably faster than that of the prototype. Both this excess speed and these initial oscillations can probably be eliminated by adjusting the spring and damping coefficients to attain a critically damped or overdamped system. This would keep the total energy of the system lower, while preventing oscillations as it converged to the final speed. Similarly, the step size on the model is smaller than that of the actual prototype.

5 Conclusion

Since the tension force in the prototype was applied from the internal motor, the forces acting on the robot will cancel and the robot will remain motionless, unless there is significant friction between the ground and the prototype. Similarly, the computer model represents this tension force by placing four separate forces at the tendon's connection points (Mass 1, Mass 2, and Mass 4). These sum to zero, and thus, create no net forward motion in the robot, yet cause all four masses to oscillate (neglecting friction). Because the motion is entirely dependent on the frictional force, the normal force (F_N) and the coefficient of friction (f_N) are the most important factors to desymmetrize to create the motion. Additionally, both the magnitude and fluctuations of the normal force are small, so the primary dependency is the coefficient of friction. In order to create a step however, the friction force must alternately prevent movement in the front and back mass. Because of the small weight of the robot, variations in the mass balance of the robot are kept small, which creates either a need for greater accuracy or for directional friction. This is easily achieved in the model, by adding three conditional `if` statements for backward, forward, or no motion. On the real prototype, directional friction was

created by adding a drop of HMA on the back side of the ring. As it was pulled in, it rotated up, lifting it barely from the ground, and when no more tension force was applied it rotated down, pushing into any smooth, hard surface. Other assymmetricalities, such as mass balance, spring constants, and damping constants seemed to have less effect on the actual motion of both the computer model and the final prototype. Nevertheless, the center of mass fluctuations were integral to both the actual and simulated motion, and had to be tuned within a margin of error to initiate the stepping motion of the robot.

6 Future Work

There are many variables that affect the motion of an amoeboid robot, including the coefficients of sliding friction (3-6), the coefficients of static friction (3-6), the directionalities of the friction coefficients (≤ 3), the damping constants (4), the spring constants (4), and the weight distribution of the robot. As a result, it was impossible to optimize the motion of the robot by manipulating the variables by hand, even with the use of force graphs and hours of trial and error. The combination of variables selected was a reasonable approximation of the actual system, with slight alterations made for improved performance, and was found by logic, guess, and experimentation. Thus, the next step in the project is to create an evolutionary optimization algorithm to balance these variables. This process will hopefully solve the issues with oscillation, excess speed, and undesired sliding that hindered the second iteration. The cost of transport or the speed could also be maximized given certain constraints on these values. Next, a reliable system of converting these theoretical values of the approximative computer model to actual, physical characteristics should be created. From here, the third, optimized amoeba prototype can be created, and its motion compared to the original.

References

[1] L. Bosgraaf and P. J. V. Haastert, *The ordered extension of pseudopodia by amoeboid cells in the absence of external cues.*, PLos ONE, 4 (2009), p. 4.

[2] M. E. Ingram and M. E. Ingram, *Whole skin locomotion inspired by amoeboid motility mechanisms*, in 29th ASME Mechanisms and Robotics Conference, 2005.

[3] T. Umedachi, K. Takeda, T. Nakagaki, R. Kobayashi, and A. Ishiguro, *A soft-bodied fluid-driven amoeboid robot inspired by plasmodium of true slime mold*, in IEEE/RSJ International Conference on Intelligent Robots and Systems, 2010.